Reprinted from September 1983, Vol. 105, Journal of Dynamic Systems, Measurement, and Control

H. Asada[2]
Assistant Professor,
Department of Mechanical Engineering,
Massachusetts Institute of Technology,
Cambridge, Mass. 02139
Assoc. Mem. ASME

T. Kanade
Senior Research Scientist,
Robotics Institute,
Carnegie-Mellon University,
Pittsburgh, Pa. 15213

I. Takeyama[2]
Kubota Ltd..
Osaka, Japan

Control of a Direct-Drive Arm[1]

A direct-drive arm is a mechanical arm in which the shafts of articulated joints are directly coupled to the rotors of motors with high torque. Since the arm does not contain transmission mechanisms between the motors and their loads, the drive system has no backlash, small friction, and high mechanical stiffness, all of which are desirable for fast, accurate, and versatile robots. First, the prototype robot is described, and basic feedback controllers for single-link drive systems are designed. Second, feedforward compensation is discussed. This compensation significantly reduces the effect of interactions among multiple joints and nonlinear forces. The experiments showed the excellent performance of the direct-drive arm in terms of speed and accuracy.

1 Introduction

As robots find more and more advanced applications, such as assembly in manufacturing, accurate, fast, and versatile manipulation becomes necessary. One of the difficulties in controlling mechanical arms is that they are highly nonlinear and involve coupling among the multiple links. Recent progress in the analysis of arm dynamics allows the real-time computation of full dynamics using efficient algorithms in a recursive Lagrangian formulation [1], a Newton-Euler formulation (2, 3], or a table look-up technique [4]. When the arm dynamics are identified accurately, the feedforward compensation of nonlinear and interactive torques combined with optimal regulators for linearized systems improves control performance greatly [5] and guarantees a global stability over a wide range of arm configurations [6].

A critical obstacle to use of dynamic models lies in the uncertainty of arm dynamics or the difficulty of identification. Even a single component in a drive system, such as a gear, a lead screw, a steel belt, or a servovalve and a pipe has complex and changeable characteristics in terms of friction, deflection, backlash, compressibility, and wear. When the arm dynamics are not well identified and subject to unknown payloads, one can use model-referenced adaptive control to maintain a uniform performance [7]. Its extensive application was shown to allow decoupling of the arm dynamics in a Cartesian coordinate system [8], the reduction on computational burdens [9], and a high speed manipulation [IO].

Alternatively, a rather straightforward way to achieve high-quality dynamic performance is to pursue the development of a new mechanism which can be modeled accurately with little difficulty. The obedient dynamical characteristics of the simplified arm may make it easy and effective to apply sophisticated control. A direct-drive arm is such a new mechanical arm which radically departs from the conventional arm mechanisms. In a direct-drive arm, unlike a conventional mechanical arm that is driven through gears, chains, and lead screws, the joint axes are directly coupled to rotors of high-torque electric motors, and therefore no transmission mechanism is included between the motors and their loads. Because of this, the drive system has excellent features, no backlash, small friction, and high stiffness. The authors have developed the first prototype of the direct-drive arm with six degrees of freedom [11]. The simple mechanism allows us to have the clear and precise model of the arm dynamics, which is of special importance not only for accurate positioning control but also for compensating interactive and nonlinear torques in high speed manipulation. This paper describes a characteristics analysis of the direct-drive arm and the design of a control system to achieve the excellent performance that the direct-drive arm potentially has.

2 Outline of the Direct-Drive Arm

The overall view of the developed direct-drive arm is shown in Photo 1 and its assembly drawing in Fig. 1. The arm has 6 degrees of freedom, all of which are articulated direct-drive joints. Beginning from the upper base frame, the first joint is a rotational joint about a vertical axis, and the second is a rotational joint about a horizontal axis. The third and fourth joints rotate the forearm about the center axis of the upper arm and about its perpendicular axis, respectively. The fifth and sixth joints perform a rotational and a bending motion of the wrist part. The total length of the arm is 1.7 m, and the movable part from joint 2 to the tip is 1 m. The movable range of joints 1 and 5 is 330 degrees. The remaining joints can move 180 degrees. The maximum payload is 6 kg including a gripper attached at the tip of the arm.

High performance d-c torque motors were used for the direct-drive arm. Photo 2 shows a bare motor at the first

[1]This work was supported by The Office of Naval Research (Contract No. N00014-81-K-0503).

[2]Formerly with Carnegie-Mellon University where this work was done.

Contributed by the Dynamics Systems and Control Division for publication in the JOURNAL OF DYNAMIC SYSTEMS, MEASUREMENT, AND CONTROL. Manuscript received by the Dynamic Systems and Control Division. May 24, 1982.

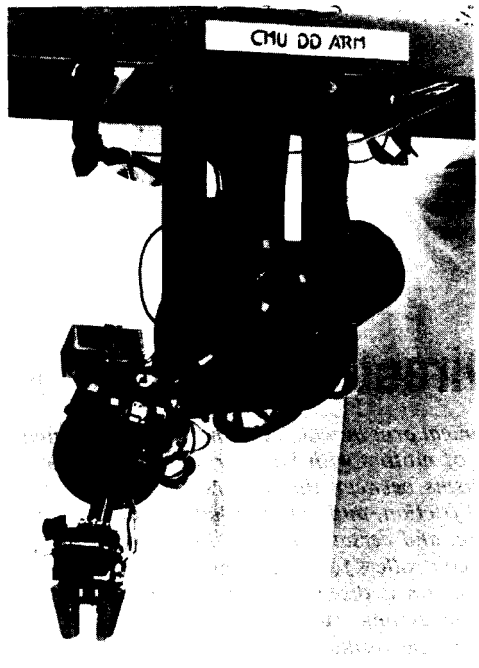

Photo 1 Overall view of direct-drive arm

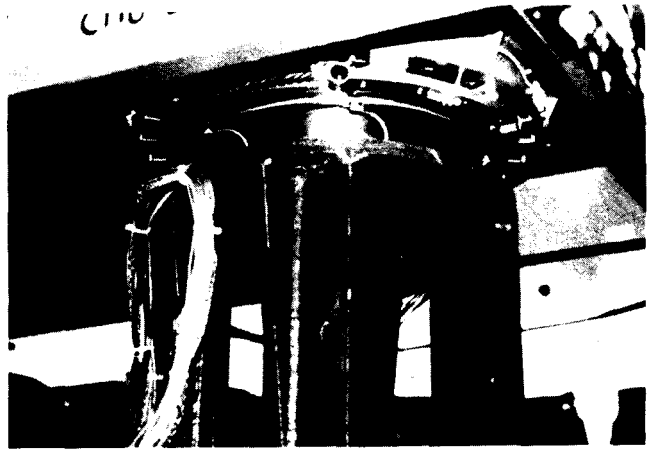

Photo 2 Bare motor at shoulder joint (joint 1)

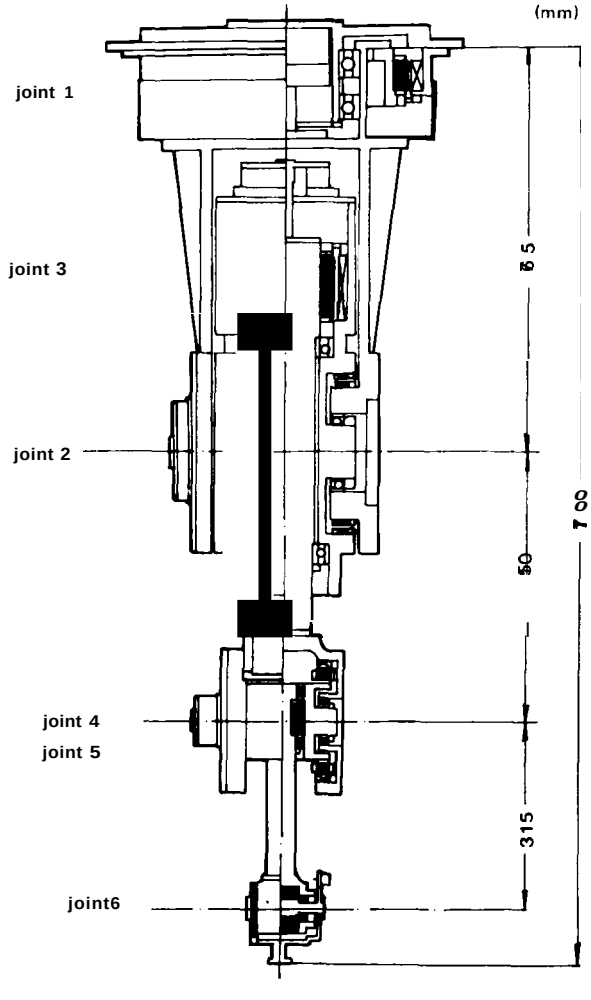

Fig. 1 Drawing of direct-drive arm

joint. The motor consists of a rotor, a stator, and a brush ring. As shown in Photo 2, each component of the motor is installed directly at the joint housing; the rotor on a hollow shaft, and the stator and the brush ring at a case. To develop a torque large enough to rotate the joint shaft directly, we selected motors with large diameters. The motor to drive joint 1 is 56 cm in diameter with 204 Nm peak torque. Joint 2 has two motors, one on each side of the upper arm. These motors are 30 cm in diameter with 136 Nm peak torque. It is required that the motors at joints 4, 5, and 6 have not only high torque but are also lightweight and compact, because heavy motors at these joints would apply a large load on upper joints. Therefore we used high performance torque motors with samarium cobalt magnets. The maximum magnetic energy product of these magnets is 3 to 10 times larger than that of conventional ferrite or alnico magnets [11]. The two samarium cobalt motors to drive joint 4 are 23 cm in diameter with 54 Nm peak torque, and the motors for the last two joints are 8 cm in diameter with 6.8 Nm peak torque.

An optical shaft encoder was installed at each joint to measure the joint angle and its angular velocity. We used precise encoders combined with accurate gears with 1 to 4 or 1 to 8 gear ratios. The resultant pulse density is 2^{16} pulses per revolution for the first four joints and 2^{15} pulses per revolution for the last two joints.

3 Mathematical Modeling and Identification

Kinematics and Dynamics. We modeled the kinematic structure of the arm according to the Denavit and Hartenberg convention [12]. The arm consists of 7 links numbered 0 to 6 from the base to the tip of the arm. Joint i is the joint that connects link i to link $i+1$. Figure 2 shows the disjointed links of the direct-drive arm where the rotors and stators of motors are disassembled and attached to separate links. Each link has a coordinate frame fixed to the link, where the z axis points the direction of the joint axis. The geometry of each link is described by the three parameters listed in Table 1. Joint displacement is given by joint angle θ_i that is the angle between the x_{i-1} and x_i axes measured in a righthand sense about z_{i-1}. The three parameters listed in Table 1 and the above joint displacement completely describe the relation between any adjacent links and the total arm configuration.

The equation of motion of the arm is derived assuming that the arm consists of a series of rigid bodies. The characteristics of a single link are completely represented by mass, center of mass, and moment of inertia about this center. We computed these parameters for each link of the direct-drive arm from the detail drawings. Table 2 shows the result, where the center

of mass and the moment of inertia are described in each link-coordinate frame.

Kinetic energy and potential energy stored into the arm are obtained by using the data listed in Tables 1 and **2.** Let joint angles θ_i and joint torques τ_i be generalized coordinates and generalized forces, respectively, then the following equation of motion is derived from substituting the kinetic and potential energies into the Lagrange's equation of motion.

$$\tau_i = \sum_{j=1}^{6} J_{ij}\ddot{\theta}_j + \sum_{j=1}^{6}\sum_{k=1}^{6} b_{ijk}\dot{\theta}_j\dot{\theta}_k + f_{gi} + f_{di} \tag{1}$$

where the first term on the right-hand side stands for inertial forces, the second term, consisting of products of angular velocities, stands for Coriolis and centrifugal forces, the third term represents gravity load, and the last term stands for the other disturbing torque such as friction and external force. The direct-drive joints have friction only at the bearings that support joint axes and at the brushes between the rotors and stators. These friction coefficients are negligibly small for most of the direct-drive joints. The parameters J_{ij}, b_{ijk}, and f_{gi} vary depending on the arm configuration, namely the functions of $\theta_1, \ldots, \theta_6$.

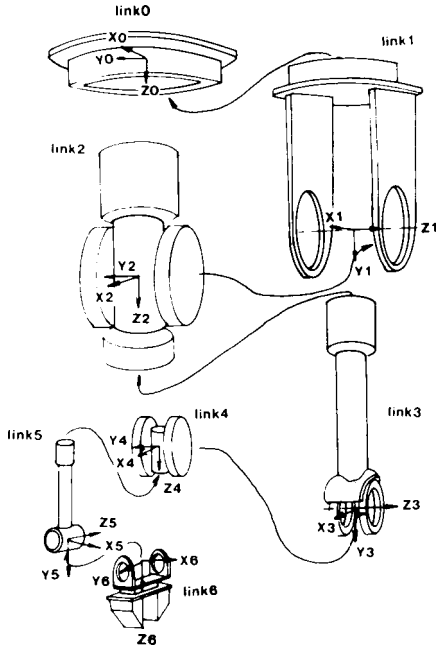

Fig. 2 Disjointed links and local coordinate frames

Drive Systems. Since the motor of a direct-drive joint is directly coupled to its joint axis, the driving torque about the axis is exactly the same as the torque developed by the motor, which is proportional to current I, applied to the motor armature;

$$\tau_i = K_{ti} I_i \tag{2}$$

where K_{ti} is torque constant. The electric characteristics of the armature are given by

$$V_i = R_i I_i + E_i \tag{3}$$

where V_i is applied voltage to the armature of the motor i, R_i is resistance of the armature, and E_i is back **EMF.** Since the inductance of the armature is small, it is neglected in the above equation. The back EMF is proportional to the angular velocity of joint axis and is given by

$$E_i = K_{ti}\dot{\theta}_i \tag{4}$$

where the back EMF constant is the same as the torque constant in metric units. Let u_i and K_{ai} be the input voltage and the voltage gain of a servo amplifier, then the characteristics equation of the drive system is derived from equations (2), (3), and **(4);**

$$\frac{K_{ai}K_{ti}}{R_i} u_i = \tau_i + \frac{K_{ti}^2}{R_i}\dot{\theta}_i \tag{5}$$

Thus the drive system is characterized by the following parameters

$$K_{ai}^* = \frac{K_{ai}K_{ti}}{R_i}, \quad C_i = \frac{K_{ti}^2}{R_i} \tag{6}$$

Table 1 Description of arm structure in Denavit and Hartenberg convention

a_i = **the distance between coordinate frames $i-1$ and i measured along x_i,**

s_i = **the distance between x_{i-1} and x_i measured along z_{i-1},**

α_i = **the angle between the z_{i-1} and z_i axes measured in a right-hand sense about x_i,**

joint #	a_i [m]	s_i [m]	α_i [deg]
1	0	0.765	180
2	0	0	-180
3	-0.035	0.510	180
4	0	0	-180
5	0	0.315	180
6	0	0	-180

Table 2 Mass, center of mass, and moment of inertia

link number	mass (kg)	center of mass (m)	moment of inertia (kgm^2)		
1	95.99	0.000 -0.675 -0.015	33.724 0.000 0.000	0.000 2.879 0.609	0.000 0.609 33.056
2	82.61	0.000 0.010 -0.203	3.990 0.000 0.001	0.000 3.786 -0.154	0.001 -0.154 1.475
3	52.90	0.029 -0.524 -0.007	8.295 0.178 -0.012	0.178 0.425 0.195	-0.012 0.195 8.237
4	13.34	-0.001 0.024 0.002	0.150 0.000 -0.001	0.000 0.062 0.001	-0.001 0.001 0.150
5	4.84	0.002 -0.176 0.000	0.110 -0.002 0.000	-0.002 0.005 0.000	0.000 0.000 0.110
6	2.81	0.000 0.008 0.032	0.016 0.000 0.000	0.000 0.011 0.002	0.000 0.002 0.006

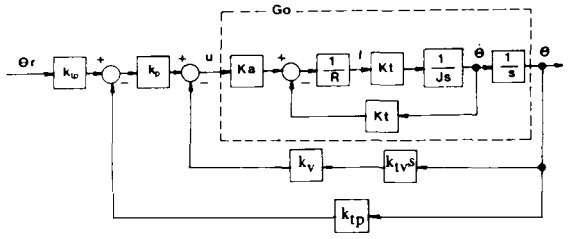

Fig. 3 Block diagram of single-link control system

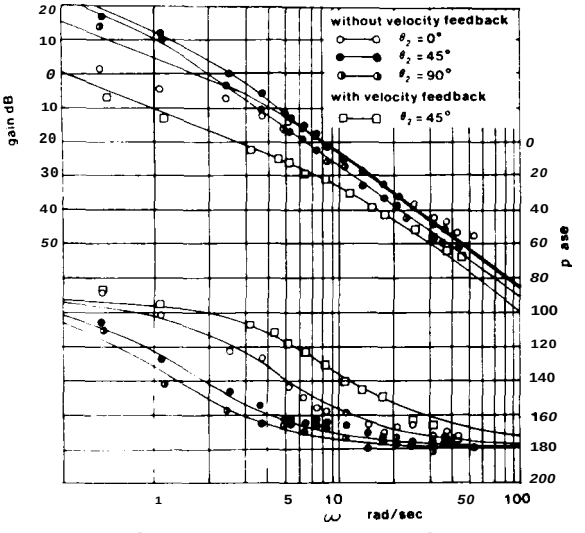

Fig. 4 Frequency response of Joint1

where K_{ai} is torque gain between the input u_i and the exerted torque τ_i, and C_i represents the coefficient of damping force inherent to the drive system. These parameters were experimentally determined. The torque gains of joints **1, 4,** and **6,** which are joints at the shoulder, elbow, and wrist of the arm, were **15.88** Nm/volt, **7.15** Nm/volt, and **2.15** Nm/volt, respectively. The coefficients of damping force of these joints were **18.17** NmS/rad, **2.31** NmS/rad, and **0.148** NmS/rad, respectively.

Single-Link Model and Frequency Response. As a first step to investigate the characteristics of servomechanisms, we assume a simplified load for each actuator. Namely, we first neglected all the nonlinear effects such as Coriolis and centrifugal forces as well as gravity and friction. We also assumed that when joint i is investigated all the other joints are mechanically immobilized. The equation of motion of the arm is then: $\tau_i = J_{ii}\theta_i$, because $\theta = 0$ and $\dot{\theta} = 0$, for $j \neq i$. Figure 3 shows the block diagram of the single-link drive system. The blocks enclosed by a broken line represent the control object including a servo amplifier, a motor, and the simplified load. The velocity feedback inside of the control object represents the back EMF of the motor. The transfer function of the control object is then given by

$$Go_i(s) = \frac{K_i}{s(T_i s + 1)}, K_i = \frac{K_{ai}^*}{C_i}, T_i = \frac{J_{ii}}{C_i} \quad (7)$$

We identified the single-link drive systems through experiments. Figures 4 and **5** show the results of frequency response for joints **1** and **4,** which are joints at the shoulder and elbow of the arm. The inertia load of each joint varies depending on the arm configuration. In particular, the inertia load on joint 1 varies remarkably relative to joint **2.** The experiments were carried out for three different arm configurations $\theta_2 = 0$, **45,** and **90** deg. Since the phase curves do not exceed **− 180** degrees for these configurations, the control object can be identified as a second-order system whose order coincides with the theoretical model just derived. The solid curves in the figures show the models derived from the parameters listed in Tables **1** and **2.** The good agreement between the models and the experimental data shows that the identified parameters were correct.

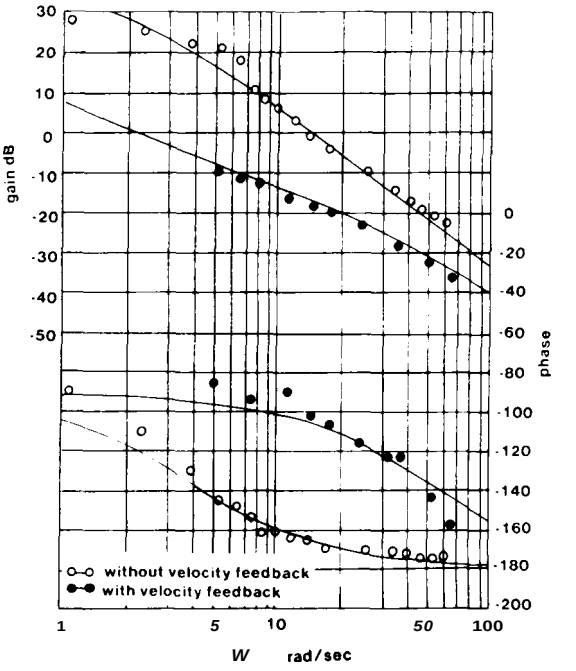

Fig. 5 Frequency response of joint 4

In general, the identification of the indirect-drive robots is more difficult because of the friction and backlash existing at the transmission mechanisms. Also, the deflection at the transmissions sometimes causes significantly large delay in higher frequency. The feature of the direct-drive robots is that it contains fewer uncertain factors and no higher-order delay. Hence the system can be identified accurately.

On the other hand, the direct-drive arm has the following problem. Let us evaluate the coefficients of damping force C_i relative to the inertia J_{ii}. From equation **(7),** the ratio of J_{ii} to C_i is the time constant of the control object. The time constants that can be determined from Figs. **4** and **5** are significantly large: T_i = **585** ms for joint **1** in case of θ_2 = **45** deg, and T_4 = **269 ms** for joint **4.** Namely, the direct-drive robot has large inertia loads relative to the damping characteristics inherent to the motors. Therefore we need to improve the damping characteristics for stabilizing the system.

4 Feedback Control

Velocity Feedback. In this section, we discuss velocity feedback to increase damping of the direct-drive joints. In the case of an indirect-drive joint, velocity is usually measured at the shaft of a motor before the speed is reduced by gears. However, it is rather difficult to do so in a direct-drive joint, because the speed of motor is as slow as the link motion. We employed high resolution shaft encoders and developed electric circuits to measure the slow speed movement of the direct-drive joint. The slowest speed that the developed system can detect was **2** deg/s for the first four joints and **4** deg/s for the last two joints. The maximum speed, on the other hand, was **180** deg/s and **360** deg/s, respectively. The resolution was **1/256** of the maximum speed in both cases.

As shown in Fig. 3, we implemented the velocity feedback

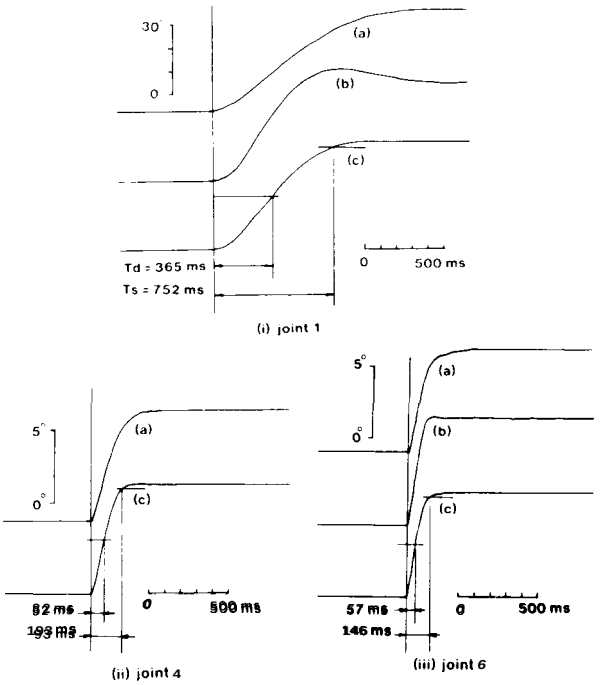

Fig. 6 Experiments of step response

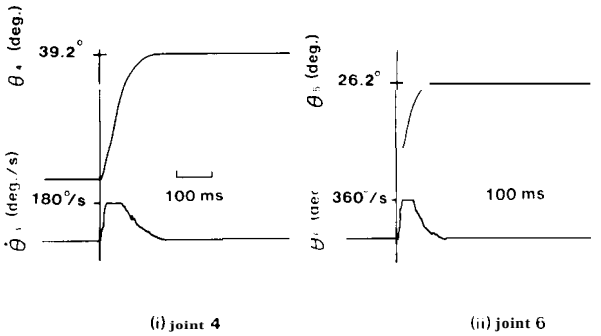

Fig. 7 Response to large step input

using the encoders, and evaluated the performance through experiments. When the velocity feedback gain Kv is increased, the damping characteristics are improved. However, if the gain is extremely large, it amplifies the error as well as the signal. When a joint rotates near the minimum detectable speed, the velocity signal varies frequently between zero and the minimum value. This varying velocity signal gives a large fluctuation of control torque and decreases control accuracy. We determined the maximum allowable gain that does not cause such a vibration, by observing the motion in slow speed control.

Figures 4 and 5 also show frequency responses of joints 1 and 4, respectively, after the velocity feedback compensation was done using the maximum allowable gains. The phase curves show a noticeable phase lead about 50 to 60 degrees. By fitting theoretical curves to the experimental data, we obtained the time constants for the improved response. The time constants of the improved systems are 92 ms and 19 ms for joints 1 and 4, respectively. The velocity feedback compensation decreases the time constants 6 to 14 times smaller than those without it.

Gain Adjustment. Now we proceed to the gain adjustment for the improved systems. Figure 3 includes a position feedback loop, where Kp is the feedback gain to be adjusted. Since overshoot is usually undesirable in the control of mechanical arms, we adjust the position feedback gain Kp so that the damping factor is between 0.9 and 1. Figure 6 shows the step response for joints 1 and 4: response (a) is overdamped, response (b) is underdamped, and response (c) is critically damped. The responses for the three joints are recorded in the same time scale. The response of joint 1, which has a large inertia load, is relatively slow, while joints 4 and 6 have very fast responses. To evaluate the transient response we used the 50 percent delay time Td and the 5 percent settling time Ts. The delay times of joints 4 and 6 were only 57 ms and 82 ms, respectively. They show that the developed direct-drive arm has excellent dynamics. Even joint 1 has a 365 ms delay time which is fast enough for most applications.

When a large step input is applied to one of the joints, the joint may be accelerated to a fast top speed for a long distance motion. However, if the joint motion is accelerated to an excessively fast speed, it is dangerous and is not desired in some applications. We modified the feedback controller so that, if the speed exceeds an allowable operating range, the velocity feedback gain is increased to several times larger than the normal operation range. Figure 7 shows the experiments of transient response for a large step input. We determined the maximum speed for joints 1 to 4 was 180 deg/s, and for joints 5 and 6, 360 deg/s. Both the joints in the figure, 4 and 6, are accelerated rapidly to the maximum speeds and settle to the reference input smoothly without overshooting. Thus the fast and stable response was achieved.

5 Feedforward Control

Control Scheme. As we analyzed in the previous section, the arm's behavior is complicated in multiple-degree-of-freedom motion. In this section, we discuss the compensation for interactive torques among multiple links and nonlinear torques such as Coriolis, centrifugal, and gravity torques. Feedforward control effectively compensates all the predictable motions, as long as the characteristics of the arm are identified accurately. The direct-drive arm has the advantage that the simple structure allows us to have the accurate model of the control object.

By solving the equation of motion inversely, we can compute the torques to drive the arm along a specified trajectory [1, 2]. Let $\theta_{r1}, \theta_{r2}, \ldots, \theta_{r6}$ be a trajectory of joint angles. If the trajectory is smooth enough to differentiate up to the second order with respect to time, the torques required to trace the trajectory with the specified speed and acceleration, θ_{ri}, θ_{ri}, are derived from equation (1)

$$\tau_{ri} = \sum_{j=1}^{6} J_{ij}(\theta_r)\ddot{\theta}_{rj} + \sum_{j,k=1}^{6} b_{ijk}(\theta_r)\dot{\theta}_{rj}\dot{\theta}_{rk} + f_{gi}(\theta_r) \quad (8)$$

where J_{ij}, b_{ijk}, and f_{gi} are functions of $\theta_{r1}, \theta_{r2}, \ldots, \theta_{r6}$. If the identification of the arm is perfect and no disturbing torque is applied to it, the arm can move along the specified trajectory with the pre-computed torques. However, as the arm travels for a long time, unavoidable errors are accumulated, even if the identification error and disturbances are small. Since coefficients involved in equation (8) are valid only when the arm configuration is in the vicinity of the predicted state, the computed torques do not make sense as errors are accumulated and the actual position of the arm diverges from the specified trajectory. Therefore we need to keep the state of the arm close to the reference trajectory. The feedback controller designed in the previous sections provides a continuous error correction of joint angles from the specified

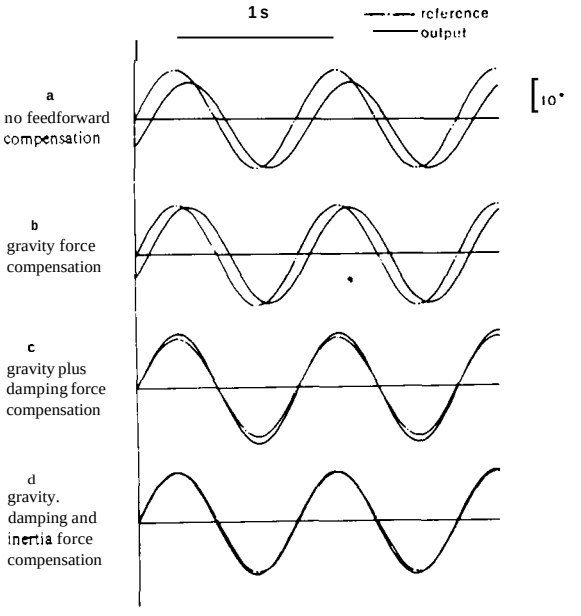

Fig. 8 Effect of feedfornard compensation for joint 4

trajectory. We extended it to a controller that can correct the error of angular velocities from their references as well as the positional errors. By combining the feedforward control with the feedback control, we expected that the former would provide the gross torques to lead the arm to a given trajectory with no delay and that the latter would provide the fine error correction to keep the state of the arm close to the reference. Thus the total torque applied to joint i is given by

$$\tau_i = \tau_{ri}(\theta_r) + Kp_i^*(\theta_{ri} - \theta_i) + Kv_i^*(\dot{\theta}_{ri} - \dot{\theta}_i) \qquad (9)$$

where Kp_i^* is forward-path gain from the position reference to the torque of motor, and Kv_i^* is the resultant velocity feedback gain including the inherent damping due to the back EMF of motor and the artificial damping through velocity feedback;

$$Kp,^* = K_{ai}^* Kp_i, Kv_i^* = C_i + K_{ai}^* Kv_i \qquad (10)$$

The second term and a part of the third term in equation (9) were already implemented in the feedback controller previously designed. Therefore, we provided the torques $\tau_{ri}(\theta_r)$ and $Kv,^*\theta_{ri}$ through a computer that solves the inverse problem of arm dynamics.

Experiments. Figure 8 shows the experimentai results of feedforward compensation for joint **4,** where the sinusoidal inputs drawn by dash-and-dot lines were given to the system as reference trajectories and its responses after settling into steady oscillations were recorded. Curve *(a)* shows the case with no compensation, where significantly large offset and phase lag were observed as well as the reduction of amplitude. Curve (*b*) shows the case with the compensation of gravity torque, where the offset vanished and the amplitude. was enlarged. In case of (*c*) where the damping torque, $Kv_i^*\theta_{ri}$, as well as the gravity torque were compensated, a remarkable improvement of phase-lag can be seen. When all the arm dynamics were taken into account, the resultant response, curve *(d),* shows excellent agreement with the reference trajectory. We observed the excellent agreements with sinusoidal inputs over wide ranges of frequency and amplitude when the driving torque, angular velocity, and joint angle did not exceed their limits.

Figure 9 shows the responses of joints **4** and *6* for sinusoidal reference trajectories. When no feedforward compensation was applied, a noticeable interaction from joint 6 to joint **4**

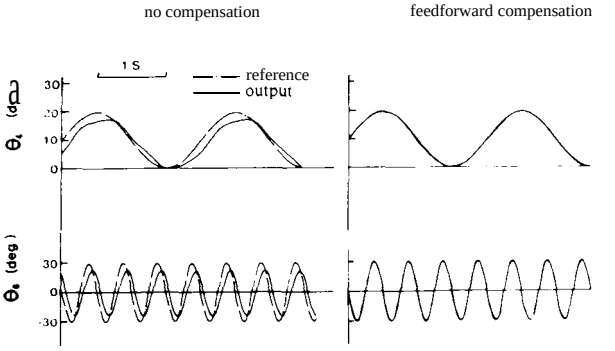

Fig. 9 Effect of feedfornard compensation for multiple joints (joints 4 and 6)

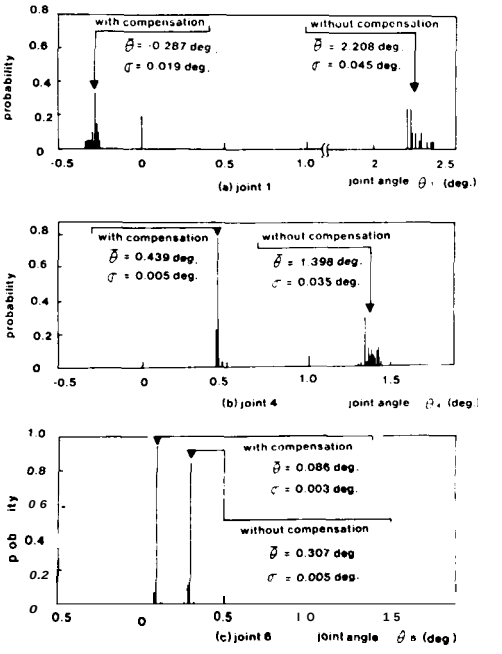

Fig. 10 Experiments of positioning accuracy

was observed. After the full dynamics of the two joints were compensated through the feedforward control, no significant interaction between them was observed and both trajectories showed excellent agreements with the references.

6 Evaluation of Steady-State Characteristics

Positioning Accuracy. In this section we evaluate the developed arm with respect to steady-state errors. Figure 10 summarizes the experiment of positioning accuracy, where the histogram of steady-state positioning errors for a step response is shown. Each histogram is obtained by more than **200** trials of the step response from the same point to the same destination. The horizontal line in each figure indicates the error from the destination (0 degree). Means and standard deviations were computed for each joint. To improve positioning accuracy, we used phase-lag compensators which increase loop gains 10 times larger in lower frequency. While joint **1,** in figure *(a),* had a large offset **2.208** deg under no compensation, it was reduced to **−0.287** deg, which **is** a reasonable error comparable to that of indirect-drive arms. However, the standard deviations indicated in the figure are very small; especially when the phase lag compensation was used, the deviation was only 0.019 deg. The other joints, joints **4** and 6, have excellent positioning performance. The small standard deviations, **0.005** deg for joint **4** and 0.003 deg

for joint 6, show that the direct-drive arm has a great advantage in terms of accuracy as well as speed. One of the reasons why the direct-drive arm shows the excellent repeatability is that the arm does not contain uncertain factors such as large friction at gears and deflection in chains and other flexible components.

Servo Stiffness. Although the direct-drive arm has fewer internal disturbances than indirect-drive arms, it is subject to external disturbances in actual operation. For example, the arm mechanically interacts with environments during manufacturing operations, or the arm grasps an unknown payload. Since these loads are not predictable in most cases, we could not compensate for them through the feedforward control discussed in the previous section.

Now we evaluate the sensitivity of the developed arm against external disturbances. Assuming that a disturbing torque Nd is applied to a joint axis, the steady-state error about this joint is $E = Nd/Kp^*$. To evaluate E we computed the deflection due to the load applied at the tip of each link. Suppose the link length is l and the disturbing force Fd is applied at the tip. Then $Fd = l \cdot Nd$, and the resultant deflection d at the tip of the link is $d = lE = l^2Fd/Kp^*$. The servo stiffness Ks of a single-link drive system is defined by the ratio of applied force Fd to the deflection d [13].

$$Ks = \frac{Fd}{d} = \frac{Kp^*}{l^2} \tag{11}$$

The servo stiffness for joints 1, 4, and 6 were 3.2 N/mm, 10.6 N/mm, and 28.8 N/mm, respectively, under the phase-lag compensation, which were comparable to the stiffness of the Stanford Manipulator [13].

7 Conclusion

This paper has presented the development of a direct-drive arm and the evaluation of its control performance. After describing the outline of the developed direct-drive arm, we derived the mathematical model of the arm. The elimination of factors which are uncertain and hard to identify, such as friction, backlash, and deflection, made it possible to develop a precise model of arm dynamics and to employ it in arm control. At the same time, the modeling enabled us to extract important issues in controlling the direct-drive arm; poor damping characteristics and significance of interactive and nonlinear forces in arm dynamics. The experiments of control of the direct-drive arm have demonstrated the solutions of the control issues. First, it was shown that sufficient damping can be provided by velocity feedback using high-precision shaft encoders. Without overshooting, the arm responded to step inputs within 60 ms to 365 ms delay time and less than 180 deg/s or 360 deg/s maximum speed. Second, the experiment was performed on feedforward compensation of arm dynamics. A remarkable improvement in dynamic performance was observed. The significance of this experiment is that we have demonstrated usefulness of feedforward compensation by being able to model the arm dynamics precisely.

References

1 Hollerbach, J. M., "A Recursive Lagrangian Formulation of Manipulator Dynamics and a Comparative Study of Dynamics Formulation Complexity," IEEE *Transaction on System, Man, and Cybernetics.* Vol. SMC-10, No. 11, Nov. 1980, pp. 730-736.

2 Luh, J. Y. S.. Walker, M. W., and Paul, R. P. C., "On-Line Computational Scheme for Mechanical Manipulators," ASME JOURNAL OF DYNAMIC SYSTEMS, MEASUREMENT, AND CONTROL, Vol. 102, No. 2, 1980, pp. 69–76.

3 Stepanenko, Y., and Vukobratovic, M., "Dynamics of Articulated Open-Chain Active Mechanisms." *Moth. Biosci.*, Vol. 28, 1976, pp. 137–170.

4 Horn, B. H. K., and Raibert. M. H., "Configuration Space Control," *The Industrial Robot,* 1978. pp. 66–73.

5 Vukobratovic, K. M., and Stokic, D. M.. "Contribution to the Decoupled Control of Large-Scale Mechanical Systems," *Automatica*, Vol. 16, Jan. 1980, pp. 9–21.

6 Vukobratovic. K. M., and Stokic. D. M., "One Engineering Concept of Dynamic Control of Manipulators," ASME JOURNM OF DYNAMIC SYSTEMS, MEASUREMENT, AND CONTROL, Vol. 102, No. 2, 1981, pp. 108–118.

7 Dubowsky, S., and DesForges, D. T., "The Application of Model-Referenced Adaptive Control to Robot Manipulators," ASME JOURNAL OF DYNAMIC SYSTEMS, MEASUREMENT, AND CONTROL, Vol. 101, No. 3, Sept. 1979, pp. 193-200.

8 Takegaki, M., and Arimoto, S., "An Adaptive Trajectory Control of Manipulators," *Int. J. of Control*, Vol. 34, No. 2, 1981, pp. 219-230.

9 Horowitz, R., and Tomozuka, M., "An Adaptive Control Scheme for Mechanical Manipulators - Compensation of Nonlinearity and Decoupling Control," ASME JOURNAL OF DYNAMIC SYSTEMS, MEASUREMENT, AND CONTROL, Vol. 1981.

10 LeBorgne, M., Ibarra, J. M., and Espiau, B., "Adaptive Control of High Velocity Manipulators," *Proc. of the 11-th Int. Symp. on Industrial Robots,* Tokyo, Oct. 1981, pp. 227-236.

11 Asada, H., and Kanade, T., "Design of Direct-Drive Mechanical Arms," ASME *Journal of Vibration. Acoustics, Stress ond Reliability in Design,* Vol. 105, No. 3, pp. 312–316, 1983.

12 Denavit, J., and Hartenberg, R. S., "A Kinematic Notation for Lower Pair Mechanisms Based on Matrices," ASME *Journal of Applied Mechanics,* June 1955, pp. 215–221.

13 Paul, R. P., "Robot Manipulators Mathematics, Programming, and Control," Chapter 7, *M. I. T. Press,* 1981.